Research Square

Preprints are preliminary reports that have not undergone peer review.
They should not be considered conclusive, used to inform clinical practice,
or referenced by the media as validated information.

Effects of boundary conditions on quantum nanoresonators: decoherence-free subspaces

Humberto C F Lemos

humbertolemos@ufsj.edu.br

Federal University of São João del-Rei

Thiago Cordeiro

Secretaria de Estado de Educação de Minas Gerais

Adelcio C Oliveira

Federal University of São João del-Rei

Research Article

Keywords: Nano-beams, Quantization, Casimir effect, Decoherence free subspace

Posted Date: May 19th, 2026

DOI: https://doi.org/10.21203/rs.3.rs-9407580/v1

License: This work is licensed under a Creative Commons Attribution 4.0 International License.
Read Full License

Additional Declarations: No competing interests reported.

Effects of boundary conditions on quantum nanoresonators: decoherence-free subspaces

Humberto C. F. Lemos,[1,*] Thiago Cordeiro,[2,†] and Adelcio C. Oliveira[1,‡]

[1] *Departamento de Estatística, Física e Matemática - CAP - Universidade Federal de São João del-Rei, Brazil.*

[2] *Secretaria de Estado de Educação de Minas Gerais. Belo Horizonte, MG, Brazil.*

(Dated: April 13, 2026)

Abstract

The Euler-Bernoulli beam model has been studied classically and semi-classically. The semi-classical quantization is done in an analogous way to the quantization of the electromagnetic field, and we found an effect that is similar to the Casimir effect, which is the photonic Casimir effect. The Casimir force, by unit area, is proportional to the first mode energy divided by the volume of the beam. For the hinged-hinged boundary condition, degenerate states were found. These degenerate pairs form decoherence-free subspaces for dispersive thermal reservoirs. For other boundary conditions, there are also subspaces with lower decoherence rates, which occur for quasi-degenerate states.

Keywords: Nano-beams, Quantization, Casimir effect, Decoherence free subspace

* Corresponding author:humbertolemos@ufsj.edu.br

† thiago.cordeiro69@educacao.mg.gov.br

‡ adelcio@ufsj.edu.br

I. INTRODUCTION

The first quantum revolution was about the building blocks of the computer, but its working functionality is as classical as that of the first mechanical computer. Now we face a second quantum revolution when the algorithm works according to quantum logic. To achieve a quantum computational advantage, we must utilize quantum properties of the system that have no classical analog. This is known as a quantum resource, and the study of this area is referred to as quantum resource theory [1]. For one-mode states, there are two resources, the negativity of the Wigner function [2] and the Squeezing [3]. While negativity is present in many applications and can be considered, in some cases, as an entanglement witness [4], non-local states signature [5, 6], and it is strongly correlated with purity. On the other hand, squeezing is an important issue to the improvement of metrology [7]. For many-mode states, the entanglement is the most used resource [8]. An important challenge, if not the most, is to keep the quantum coherence [9]; thus, it is important to know what makes the system behave classically. A quantum system behaves classically due to a combination of three factors: large actions, interaction with the environment, and measurement disturbance [10, 11]. To avoid these troubles, small actions are usually considered, and many different strategies of measurement, such as non-demolition measurements [12] and weak interactions [13]. The interaction with the environment depends on the particular experimental realization, with large advances in many areas [14–16].

Nanomechanical beams are mechanical structures that can be fabricated [17]. They serve as useful models for nanotubes [18] and microtubules [19–21], and have various applications [22]. There is also significant interest in the quantum properties of these systems, with numerous studies exploring their quantum effects and applications [23–26], as well as investigations into philosophical questions such as consciousness [27]. In the classical domain, these mechanical systems exhibit rich dynamics, including chaotic behavior [28–38] and stochastic dynamics [39].

Due to the large number of particles, modeling a nanoresonator or a nanobeam is not a simple task. Classical models limit their treatment as a continuous medium, and discrete aspects of the material's lattice may be relevant. Among the approaches is atomic modeling, which essentially involves solving the Schrödinger equation for a system of N atoms. Atomic modeling is usually divided into molecular dynamics, Monte Carlo, density functional theory,

tight bonding molecular dynamics, local density, Morse potential function model, and ab initio approaches [40].

In this work, we will investigate the continuum model [40], based on the Euler-Bernoulli beam model. Continuum models have already been studied in several other works [40–42]; here, our interest is in semiclassical modeling and how boundary conditions affect the dynamic behavior of the quantum nanobeam.

The classical and consequently, the quantum solutions of the nanobeams are strongly affected by the contour conditions, and while boundary conditions are extensively investigated in classical domains, there are few attempts to capture its effects in the quantum domain [43]. In our model, different boundary conditions imply in significantly different sensitivity of environmental action, suggesting the existence of decoherence-free subspaces [44–46]. The work is organized as follows: in II we briefly review the theoretical modeling of classical beams. In section III, we investigate the quantum version for the clamped-clamped, clamped-hinged, and clamped-free boundaries. In section IV we investigate the possible existence of decoherence-free subspaces for phase damping reservoir [47, 48]. In section V we present our conclusions.

II. CLASSICAL BEAM MODELING

We begin by studying the behavior of an elastic beam under small transverse vibrations, subjected to different loads and under different boundary conditions. Consider a beam of length L as illustrated in figure 1: the reader may notice that the reference frame is set such that the x-axis runs along the span of the beam.

We briefly summarize the main results from the Euler-Bernoulli beam theory, with detailed discussions available in standard textbooks, such as [49]. We assume that the beam's displacements are confined to the xz-plane and denote them by $w(x,t)$, where positive w indicates downward displacement. The potential energy of the beam is given by

$$U(t) = \frac{1}{2}\int_0^L EI\left(\frac{\partial^2 w}{\partial x^2}\right)^2 dx, \tag{1}$$

where E is the Young's modulus of the material, and I represents the area moment of inertia of the beam's cross-section about the y-axis. The kinetic energy of the beam is

$$T(t) = \frac{1}{2}\int_0^L \rho A\left(\frac{\partial w}{\partial t}\right)^2 dx, \tag{2}$$

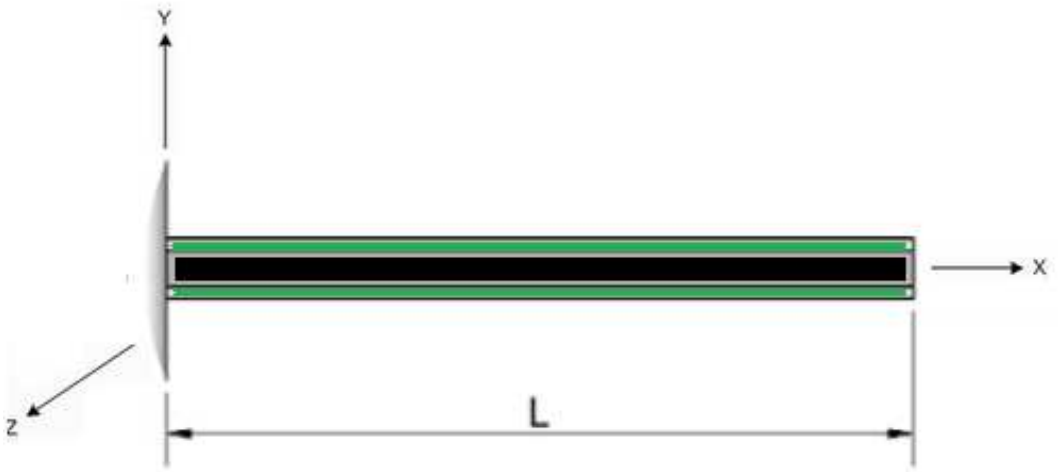


FIG. 1. Euler-Bernoulli beam schematic model.

where ρ is the mass density of the beam and A is the cross-sectional area of the beam about the y-axis.

Applying the energies derived above, the Lagrangian mechanics formalism yields a general equation for the beam's behavior, as detailed in [49]. The analysis initially considers a homogeneous beam with a uniform cross-section along its length. It is further assumed that no axial load acts along the beam and that the beam does not rest on an elastic foundation. Under these conditions, the vertical deflection w as a function of horizontal position x and time t is governed by the following fourth-order linear non-homogeneous partial differential equation (PDE):

$$EI\frac{\partial^4 w}{\partial x^4} + \rho A\frac{\partial^2 w}{\partial t^2} = f(x,t), \tag{3}$$

for $0 < x < L$, where f represents an external transversal loading per unit length of the beam. To find the general solutions for this equation, we first consider the homogeneous case where $f = 0$. This homogeneous PDE can be solved using the method of separation of variables. We assume the solution takes the form $w(x,t) = \xi(x)\tau(t)$, with the precise form of the spatial solution depending on the boundary conditions. There are many known boundary conditions for this problem [49]. For our initial study, we consider the hinged-hinged case, leading to the boundary conditions

$$w = 0\ , \quad \text{and} \quad \frac{\partial^2 w}{\partial x^2} = 0, \tag{4}$$

at both boundaries of the beam, namely at $x = 0$ and $x = L$. Alternative boundary

conditions are discussed in a subsequent section.

The partial differential equation (PDE) (3) can be separated into two linear ordinary differential equations (ODEs):

$$\xi^{(4)}(x) - \lambda^4 \xi(x) = 0, \tag{5a}$$

$$\ddot{\tau}(t) + \frac{\rho A}{EI}\,\lambda^4 \tau(t) = 0. \tag{5b}$$

By applying the boundary conditions (4) to Eq. (5a), we can determine the eigenvalues λ, which correspond to the normal modes of the beam

$$\lambda_k = \frac{k\pi}{L}, \quad k = 1, 2, \ldots, \tag{6}$$

with the spatial solutions given by the eigenfunctions

$$\xi_k(x) = \sin(\lambda_k x), \tag{7}$$

for $k \geq 1$. It is important to note that different boundary conditions yield distinct normal modes. The hinged-hinged case is analytically tractable and serves as a useful example, although it is challenging to implement in a nanometer-scale experimental apparatus due to the analytical determination of frequencies. The vibrational modes of the beam are examined in greater detail in subsection III C, where the implications of this choice are discussed. Under the boundary conditions (4), the beam equation (3) admits an infinite number of solutions, resulting in the well-known general solution:

$$w(x,t) = \sum_{k\geq 1} w_k(x,t) = \sum_{k\geq 1} \tau_k(t) \sin(\lambda_k x). \tag{8}$$

Once the eigenvalues are determined, solving Eq. (5b) for each $k \geq 1$ becomes straightforward, as it reduces to the equation of a harmonic oscillator with a natural frequency given by

$$\omega_k = \sqrt{\frac{\rho A}{EI}}\,\lambda_k^2 = \sqrt{\frac{\rho A}{EI}}\,\left(\frac{k\pi}{L}\right)^2. \tag{9}$$

The solution for Eq. (5b) is widely known. If initial conditions for the beam were provided, the complete classical solution $w(x,t)$ could be determined. However, we are not interested in solving the classic beam problem, as this has already been thoroughly explored. Instead, we will proceed with the quantization of these harmonic oscillators to study nanoresonators.

III. QUANTIZATION: SEMICLASSICAL APPROACH

We now proceed to the next step: the quantization of the beam. Specifically, we use the classical solution for the spatial part of the problem, given by the eigenfunctions (7). As discussed in Section II, the temporal counterpart is described by an infinite set of harmonic oscillators, each corresponding to a different mode $k \geq 1$ in Eq. (5b). To study the quantum behavior of the system, we take the quantum version of these oscillators. Here, we consider that the beam is composed of countless particles, thousands or more. These nano-beams can, in fact, be monitored in real time, with their collective position and momentum measured almost constantly. Thus, we assume that the continuous monitoring regime has been reached [11], and that Newtonian dynamics is valid. However, continuous monitoring does not affect the spectrum of the Hamiltonian, so the temporal part is treated by a quantum in order to obtain part of the energy levels.

The quantum harmonic oscillator is a well-established problem, making its quantization straightforward. However, to validate our approach, we first evaluate the total energy of the beam. Substituting the general solution (8) into the potential energy expression (1), and using the orthogonality of the eigenfunctions (7), the potential energy of the beam is found to be

$$U(t) = \sum_{k\geq 1} \frac{EIL}{4}\, \lambda_k^4 \tau_k^2(t),$$

Similarly, the kinetic energy is given by

$$T(t) = \sum_{k\geq 1} \frac{\rho AL}{4}\, \dot{\tau}_k^2(t).$$

Thus, the total energy of the beam, expressed as the Hamiltonian, is

$$\mathcal{H}(t) = \sum_{k\geq 1} \frac{1}{2}\, \frac{\rho AL}{2}\, \dot{\tau}_k^2(t) + \frac{1}{2}\, \frac{EIL}{2}\, \lambda_k^4 \tau_k^2(t). \tag{10}$$

This Hamiltonian is precisely that of an infinite set of decoupled harmonic oscillators, one for each mode $k \geq 1$. We define the generalized coordinates as $q_k(t) = \tau_k(t)$, therefore the generalized velocities are $\dot{q}_k(t) = \dot{\tau}_k(t)$. The first term in the summation, representing the kinetic energy, can be recognized as that of a harmonic oscillator with mass $m = \rho AL/2$. Such identification is two-fold: firstly, the potential energy term can be rewritten as

$$U(t) = \sum_{k\geq 1} \frac{1}{2}\, \frac{\rho AL}{2}\, \frac{EI}{\rho A}\, \lambda_k^4 \tau_k^2(t) = \sum_{k\geq 1} \frac{1}{2}\, m\omega_k^2 q_k(t),$$

which corresponds to the potential energy of a harmonic oscillator with mass m and frequency ω_k given by (9). Additionally, if we define the generalized momenta as $p_k(t) = (\dot{\tau}_k(t)/m)$, the Hamiltonian can be rewritten as

$$\mathcal{H}(t) = \sum_{k\geq 1} \frac{1}{2}\frac{p_k^2(t)}{m} + \frac{1}{2}\, m\omega_k^2 q_k(t). \tag{11}$$

With this formulation, we are ready for quantization. The total energy (10) is replaced by the Hamiltonian operator $\hat{\mathcal{H}}$. Correspondingly, position and momentum are replaced by the operators $\hat{q}_k$ and $\hat{p}_k$, which satisfy the canonical commutation relations. We define the annihilation and creation operators, $\hat{a}_k$ and $\hat{a}_k^\dagger$, respectively, as

$$\hat{a}_k = \sqrt{\frac{m\omega_k}{2\hbar}}\left(\hat{q}_k + \frac{i}{m\omega_k}\hat{p}_k\right), \tag{12a}$$

$$\hat{a}_k^\dagger = \sqrt{\frac{m\omega_k}{2\hbar}}\left(\hat{q}_k - \frac{i}{m\omega_k}\hat{p}_k\right). \tag{12b}$$

These operators satisfy the commutation relations

$$[\hat{a}_k, \hat{a}_{k'}] = 0 = [\hat{a}_k^\dagger, \hat{a}_{k'}^\dagger], \quad [\hat{a}_k, \hat{a}_{k'}^\dagger] = \delta_{k,k'}. \tag{13}$$

For each $k \geq 1$, the number operator is $\hat{N}_k = \hat{a}_k^\dagger \hat{a}_k$, and so the Hamiltonian is

$$\hat{\mathcal{H}} = \sum_{k\geq 1} \hat{\mathcal{H}}_k = \sum_{k\geq 1} \hbar\omega_k \left(\hat{N}_k + \frac{1}{2}\right), \tag{14}$$

where $\hat{\mathcal{H}}_k = \hbar\omega_k(\hat{N}_k + 1/2)$ is the Hamiltonian for each k.

As expected, the number operator $\hat{N}_k$ satisfies the commutation relations

$$[\hat{N}_k, \hat{a}_{k'}] = -\hat{a}_k\delta_{k,k'}, \quad [\hat{N}_k, \hat{a}_{k'}^\dagger] = \hat{a}_k^\dagger\delta_{k,k'}.$$

Moreover, for each $k \geq 1$ and for each $n \geq 0$, the state $|k, n\rangle$ is an eigenvector of $\hat{N}_k$, with eigenvalue $\hat{N}_k\,|k,n\rangle = n\,|k,n\rangle$. Consequently, it is an eigenvector for $\hat{\mathcal{H}}_k$, i.e. $\hat{\mathcal{H}}_k\,|k,n\rangle = \varepsilon_{k,n}\,|k,n\rangle$, and its eigenenergy is given by

$$\varepsilon_{k,n} = \hbar\omega_k\left(n + \frac{1}{2}\right) = \frac{\hbar\pi^2}{L^2}\sqrt{\frac{\rho A}{EI}}\,k^2\left(n + \frac{1}{2}\right). \tag{15}$$

At this stage, the model is considered solved in a formal sense. However, we will now delve deeper into specific aspects to further analyze the implications of our findings.

A. Renormalization

Lets consider $k \geq 1$ and $n \geq 0$, we can write $\varepsilon_{k,n}$ as

$$\varepsilon_{k,n} = Ck^2 \left(n + \frac{1}{2} \right), \tag{16}$$

and C is defined by (15). The vacuum energy is $\varepsilon_{k,0} = Ck^2/2$, thus considering all states, the sum $\sum_k \varepsilon_{k,n}$ is divergent.

Now defining a "re-normalized"mode energy as

$$\varepsilon^{(0)}_{k,n} = Ck^2 n. \tag{17}$$

we have $\varepsilon^{(0)}_{k,0} = 0$, also

$$\varepsilon_{k,n} = \varepsilon^{(0)}_{k,n} + \frac{Ck^2}{2} = \varepsilon^{(0)}_{k,n} + \varepsilon_{k,0}.$$

When we write $\hat{\mathcal{H}}_k$ it is a compact way to say that

$$\hat{\mathcal{H}}_k = \underbrace{I \otimes \ldots \otimes I}_{(k-1) \text{ times}} \otimes \hat{\mathcal{H}}_k \otimes I \ldots, \tag{18}$$

and the state $|k, n\rangle$ represents the state

$$|k, n\rangle = |1, 0\rangle \otimes \ldots |k-1, 0\rangle \otimes |k, n\rangle \otimes |k+1, 0\rangle \otimes \ldots. \tag{19}$$

The eigenvalue eigenvector equation given by $\hat{\mathcal{H}} |k, n\rangle = E_{k,n} |k, n\rangle$, where the energy eigenvalues $E_{k,n}$ are given by

$$E_{k,n} = \sum_{j \geq 1; j \neq k} \varepsilon_{j,0} + \varepsilon_{k,n}. \tag{20}$$

Similarly, we can define the renormalized case $E^{(0)}_{k,n} = \varepsilon^{(0)}_{k,n}$. Important to note that

$$E_{k,0} = \frac{C}{2} \sum_{j \geq 1} k^2 = \infty. \tag{21}$$

This problem clearly does not exist for the renormalized energy $E^{(0)}_{k,n}$. From now on, we use the renormalized energy, in a similar approach to the electromagnetic field [50]. In the electromagnetic field, this zero-point energy can be observed in an experimental situation as the Casimir effect.

B. Effects of vacuum: The Phonon Casimir Effect

The vacuum non-normalized energy is given by

$$E_{k,0} = \sum_k \frac{1}{2}\hbar\omega_k,$$

Here we assume an analogous approach of electromagnetic [50] field to obtain the action of vacuum on beam, this is the phonon Casimir effect [51–54].

$$\omega_k = \sqrt{\frac{\rho A}{EI}}\left(\frac{k\pi}{L}\right)^2 = \tilde{\omega}k^2.$$

We can also write it as a function of sound speed, in a solid, it is

$$v = \sqrt{\frac{E}{\rho}}$$

then

$$\omega_k \;=\; \frac{1}{v}\sqrt{\frac{A}{I}}\left(\frac{\pi}{L}\right)^2 k^2. \tag{22}$$

Finally, we can write the zero-point phonon energy as

$$E_{k,0} = \frac{1}{v}\hbar\sqrt{\frac{A}{I}}\left(\frac{\pi}{L}\right)^2 \sum_{k=1}^{\infty} k^2.$$

If we consider a free system, without k restriction, then

$$E_f = \frac{1}{v}\hbar\sqrt{\frac{A}{I}}\left(\frac{\pi}{L}\right)^2 \int_0^{\infty} k^2 dk. \tag{23}$$

The difference $\Delta E = E_{k,0} - E_f$ is

$$\Delta E = E_{k,0} - E_f = \frac{1}{v}\hbar\sqrt{\frac{A}{I}}\left(\frac{\pi}{L}\right)^2 \left[\sum_{k=1}^{\infty} k^2 - \int_0^{\infty} k^2 dk\right]. \tag{24}$$

Using a normalizing factor $e^{-\varepsilon k^2}$, we have

$$\begin{aligned}\Delta E \;&=\; E_0 - E_f = \frac{1}{v}\sqrt{\frac{A}{I}}\left(\frac{\pi}{L}\right)^2 \hbar \lim_{M\to\infty,\varepsilon\to 0}\left[\sum_{k=1}^{M} k^2 e^{-\varepsilon k^2} - \int_0^{M} k^2 e^{-\varepsilon k^2} dk\right] \\ &=\; \frac{1}{v}\sqrt{\frac{A}{I}}\left(\frac{\pi}{L}\right)^2 \hbar \lim_{M\to\infty,\varepsilon\to 0}\left\{-\frac{d}{d\varepsilon}\left[\sum_{k=1}^{M} e^{-\varepsilon k^2} - \int_0^{M} e^{-\varepsilon k^2} dk\right]\right\}\end{aligned} \tag{25}$$

Observing that

$$\int_1^M e^{-\varepsilon k^2} dk < \sum_{k=1}^{M} e^{-\varepsilon k^2} < \int_0^M e^{-\varepsilon k^2} dk,$$

then, for a sufficiently small ε we have

$$\sum_{k=1}^{M} e^{-\varepsilon k^2} \approx \frac{1}{2}\left(\int_1^M e^{-\varepsilon k^2} dk + \int_0^M e^{-\varepsilon k^2} dk\right)$$

or

$$\sum_{k=1}^{M} e^{-\varepsilon k^2} - \int_0^M e^{-\varepsilon k^2} dk \;\approx\; -\frac{1}{2}\int_0^1 e^{-\varepsilon k^2} dk \tag{26}$$

Now, inserting (26) into (25) we have

$$\Delta E \;\approx\; \frac{1}{v}\sqrt{\frac{A}{I}}\left(\frac{\pi}{L}\right)^2 \hbar \lim_{M\to\infty}\lim_{\varepsilon\to 0}\left\{-\frac{d}{d\varepsilon}\left[-\frac{1}{2}\int_0^1 e^{-\varepsilon k^2} dk\right]\right\} \tag{27}$$

$$= -\frac{1}{2}\frac{1}{v}\sqrt{\frac{A}{I}}\left(\frac{\pi}{L}\right)^2 \hbar\left\{\int_0^1 k^2\, dk\right\} \tag{28}$$

$$= -\frac{1}{6}\frac{1}{v}\sqrt{\frac{A}{I}}\left(\frac{\pi}{L}\right)^2 \hbar. \tag{29}$$

Finally we obtain

$$\Delta E \approx -\frac{1}{6}\frac{1}{v}\hbar\sqrt{\frac{A}{I}}\left(\frac{\pi}{L}\right)^2 = -\frac{1}{6}\hbar\sqrt{\frac{\rho A}{EI}}\left(\frac{\pi}{L}\right)^2. \tag{30}$$

Now the energy per area ($\mathcal{V}$) acting in the beam cross section is

$$\mathcal{V} \approx -\frac{1}{6}\frac{1}{v}\hbar\sqrt{\frac{1}{IA}}\left(\frac{\pi}{L}\right)^2 = -\frac{1}{6}\hbar\sqrt{\frac{\rho}{EIA}}\left(\frac{\pi}{L}\right)^2, \tag{31}$$

and thus the force per unit area $F = -\frac{\partial \mathcal{V}}{\partial L}$, is

$$F \approx -\frac{1}{3}\hbar\sqrt{\frac{\rho}{EIA}}\frac{\pi^2}{L^3} = -\frac{1}{3}\frac{1}{AL}\hbar\tilde{\omega}. \tag{32}$$

Note from (32) that $F \propto L^{-3}$, and it is proportional to the energy fundamental state of the first mode, $k = 1$, divided by the volume of the beam. A discussion of a similar phonon Casimir effect can be found in references [51, 52]. Consequently, it is very small and attractive. In the next calculations, we will neglect this force. On the other hand, if the term AL is small and F isn't negligible, the force F should be considered from the beginning in the Euler-Bernoulli modeling [55].

C. Degeneracy and effects of boundary conditions

In this subsection, we investigate if this model presents energy degeneracy, i.e. for which values for the pairs of indices $(k,n) \neq (k',n')$ we could have $E_{k,n} = E_{k',n'}$. First, we observe that

$$\begin{aligned} E_{k,n} - E_{k',n'} &= \left(\sum_{j\neq k} \varepsilon_{j,0} + \varepsilon_{k,n}\right) - \left(\sum_{j\neq k'} \varepsilon_{j,0} + \varepsilon_{k',n'}\right) = \\ &= (\varepsilon_{k,n} + \varepsilon_{k',0}) - (\varepsilon_{k',n'} + \varepsilon_{k,0}) = \\ &= (\varepsilon_{k,n} - \varepsilon_{k,0}) - (\varepsilon_{k',n'} - \varepsilon_{k',0}) = \\ &= \varepsilon^{(0)}_{k,n} - \varepsilon^{(0)}_{k',n'} = E^{(0)}_{k,n} - E^{(0)}_{k',n'}. \end{aligned}$$

Therefore we have $E_{k,n} = E_{k',n'}$ if, and only if, $\varepsilon^{(0)}_{k,n} = \varepsilon^{(0)}_{k',n'}$, and consequently

$$Ck^2 n = C(k')^2 n' \Rightarrow n = \left(\frac{k'}{k}\right)^2 n'. \tag{33}$$

For instance, if $k' = 2k$, then $n = 4n'$, a particular case is $E_{1,4} = E_{2,1}$.

Experimentally, the boundary conditions have an impact on the quality factor of the resonator Q^{-1}. Takamura and collaborators [56] have observed different Q^{-1} for free-free edges and doubly clamped graphene resonators. A dependence of Q^{-1} on the boundary conditions has also been found in classical molecular dynamics simulations [57]. In reference [58], they found a fitting for the decay rate as $e^{-\eta\omega t}$, where η is a constant and ω is the natural beam frequency.

In our model, the boundary determines λ_k and consequently ω_0; the value of λ_k given by 6 is found for the hinged-hinged boundary condition; for other boundary conditions, it does not have such a simple analytical formula. The degeneracy, found in the previous section, only exists because the ratio between two consecutive values of λ_k is a rational number. Let us now analyze other possibilities that can be found in real situations, namely, clamped-clamped, clamped-hinged, clamped-free, and free-free. The solution (6) is obtained by the roots of the characteristic equation $F_0(\lambda_k L) = \sin(\lambda_k L)$; for other boundary conditions, we have different characteristic equations given in table I.

In figure 2 we see the first roots of F_1, F_2 and F_3. They differ little from the roots of F_0, the hinged-hinged case, which is evident in figure 3 where ω_0 refers to the hinged-hinged case. Considering the functions F_j, for $j \neq 0$, we have for small values of k the difference

clamped-clamped	$F_1(x) = \cos x \cosh x - 1$
clamped-hinged	$F_2(x) = \cos x \sinh x - \sin x \cosh x$
clamped-free	$F_3(x) = \cos x \cosh x + 1$
free-free	$F_4(x) = \cos x \cosh x - 1 = F_1(x)$

TABLE I. Characteristic Equation for determining λ_k for different boundary conditions, and $x = \lambda_k L$.

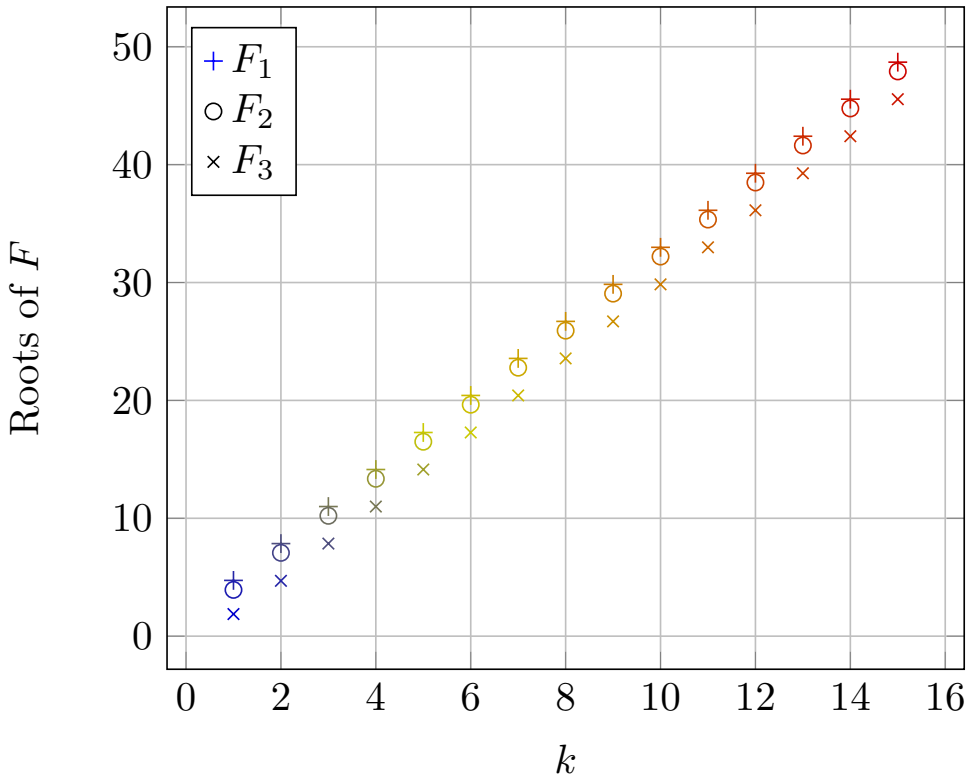


FIG. 2. Roots of F_j as function of k for $L = 1$.

$\lambda_{k+1} - \lambda_k$ has no simple relation to π, this for all functions $F_m(x)$, and $m = 1, ..., 4$. For $k > 4$ we have that $\frac{\lambda_{k+1}-\lambda_k}{\pi L} \approx 1$, and $\lambda_k L \approx q\pi$ where $q \in \mathbb{Q}$. For $k > 10$ we have that $\frac{\lambda_{k+1}-\lambda_k}{\pi L} = 1 + \epsilon$ and $|\epsilon| \leq 10^{-13}$.

Thus, for larger values of k, there will always be a quasi-degeneracy, which in an experiment may be difficult to differentiate from a real degeneracy.

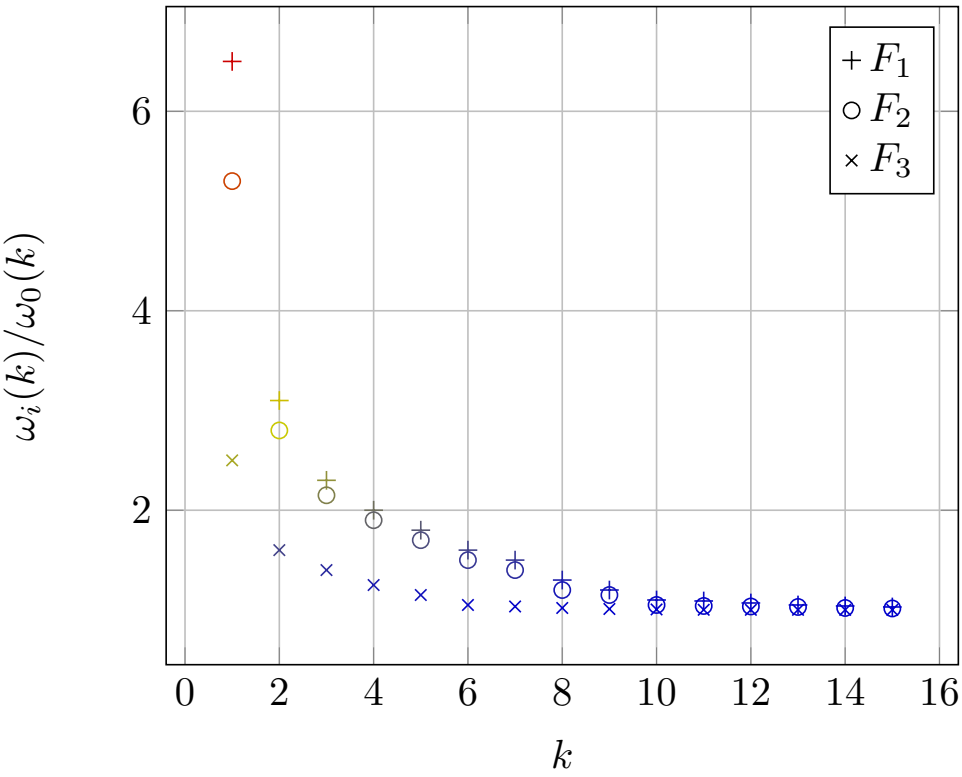


FIG. 3. Ratio of $\frac{\omega_i}{\omega_0}$ as function of k, and $\omega_0(k) = \frac{\pi^2}{L^2}\sqrt{\frac{\rho A}{EI}}\,k^2$.

IV. DECOHERENCE "FREE" SUBSPACE

Now we consider that the beam is not isolated, but it is connected by its surroundings interacting by inelastic collisions, or, in other words, there is no energy exchange. This is the phase-dumping reservoir [47]. We consider a reservoir model with a large number of harmonic oscillators. On the other hand, the effectiveness of the phase dumping reservoir depends solely on the effective Hilbert space [48]. The Hamiltonian for the total system environment is given by

$$\hat{H} = \hat{H}_S + \hat{H}_I + \hat{H}_E, \tag{34}$$

where

$$\hat{H}_S = \sum_k \hat{\mathcal{H}}_k, \tag{35}$$

$$\hat{H}_I = \lambda \sum_{k,j} \hat{\mathcal{H}}_k b_j^\dagger b_j, \tag{36}$$

and

$$\hat{H}_E = \sum_j \omega_j b_j^\dagger b_j. \tag{37}$$

Here λ is a coupling constant, b_k ($b^\dagger$) is the destruction (creation) operator of the k-th environment oscillator, and ω is its frequency. We will consider only two modes, then $\hat{H}_S = \hat{\mathcal{H}}_j + \hat{\mathcal{H}}_k$. The eigenstates of $\hat{H}_S$ are now of the form

$$\hat{H}_S \left|\phi_{m,n}\right\rangle = \hat{H}_S \left|m,n\right\rangle = E_{m,n} \left|m,n\right\rangle, \tag{38}$$

where $E_{m,n} = \hbar\omega_j m + \hbar\omega_k n$. The time evolution of states in this basis can be obtained by

$$\left|\phi_{m,n}\right\rangle \left\langle\phi_{m',n'}\right| (t) = e^{-\left[\Lambda(\overline{n})(\Delta E)^2\right]t} \left|\phi_{m,n}\right\rangle \left\langle\phi_{m',n'}\right|, \tag{39}$$

where $\Delta E = E_{m,n} - E_{m',n'}$ and $\Lambda(\overline{n})$ is a function of the mean photon number of the environment $\overline{n}$, and the coupling constant λ, see [47, 48] for details. The diagonal states are not affected by the phase dumping reservoir, since $\Delta E = 0$, but not only the diagonal states. Let's consider the state

$$\left|\psi_D\right\rangle = a \left|0\right\rangle_j \otimes \left|n\right\rangle_k + b \left|m\right\rangle_j \otimes \left|0\right\rangle_k, \tag{40}$$

and we assume that the state $\left|0\right\rangle_j \otimes \left|n\right\rangle_k$ and $\left|m\right\rangle_j \otimes \left|0\right\rangle_k$ are degenerate, then $\left|\psi_D\right\rangle$ is preserved. If the contour condition is not hinged-hinged, then there is no degeneracy and the state is not preserved, but, as previously discussed, there are some pairs that are nearly degenerated. In this condition, the state is not preserved, but it has a greater lifetime. In figure 4, we plot the linear entropy δ that is defined as $\delta = 1 - \mathrm{Tr}\{\rho^2\}$ for the state 40 in a clamped-hinged contour condition. As we can see, there is a large variation in the decoherence time. In a phase-damping reservoir, the decoherence time usually depends on the difference in the energy levels. Here, the difference lies in the fact that the energy levels are not equally spaced if we consider two or more modes. The natural choice would be $(j,m) = (1,1)$ and $(k,n) = (2,1)$, but the biggest decoherence time was found for $(j,m) = (1,2)$ and $(k,n) = (2,1)$. For larger values of k we have that $\omega_k \approx \omega_0(1)(k + \frac{1}{4})^2$. The factor $\frac{1}{4}$ in ω_k drives the "degeneracy" to larger values of m and n, although the energy difference becomes proportionally smaller; in fact, it is not small, and those states are not less affected by the environment.

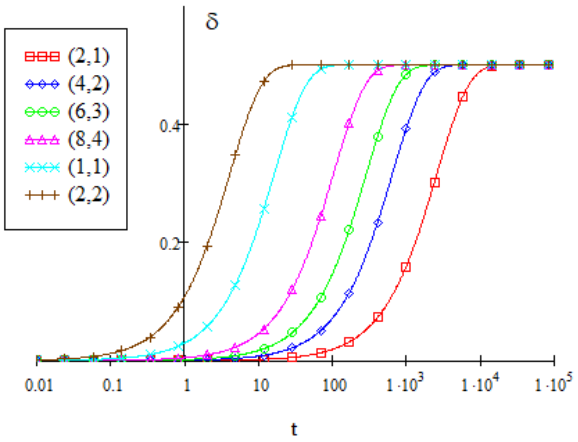


FIG. 4. Time evolution of linear entropy of the state 40 for $a = b = \frac{1}{\sqrt{2}}$, $j = 1$ and $k = 2$. The values of (m, n) are given in the legend. The others constants are chosen as $\frac{\rho A}{EI} = 1$, $\hbar = 1$, and $\Lambda = \frac{1}{(10\pi)^2}$. The beam contour condition is clamped-hinged.

1. *Some considerations about a more realistic thermal bath*

If we consider a zero-temperature thermal bath [59], we have a decay rate that depends on $D(\omega)d\omega$, which represents the number of modes in the frequency interval between ω and $\omega + d\omega$ of the thermal bath. Since the modes represent vibrational states of the same beam, the density of states of the thermal bath is the same. However, since different vibration modes represent deformations with different wavelengths, it is reasonable to imagine that the coupling between the baths must be different for each vibrational mode, and therefore the rates of loss of coherence (κ_i) can be very different, where κ_i is the decay rate of the vibrational mode i. If we assume that the decay rate is $\kappa = \eta\omega$ as shown in ref. [58], then we can have $\kappa_A \ll \kappa_B$. If the modes were uncoupled, the mode B would lose its coherence much faster than mode A. Now, including a coupling, it makes them decay at a rate κ_{AB}, and we have $\kappa_{AB} \approx \kappa_A$, which is a necessary condition for the existence of a decoherence-free subspace [59]. In this case, it is not a subspace without decoherence but one with a significantly longer half-life.

V. CONCLUSIONS

As we can see, the semiclassical treatment of the Euler-Bernoulli nanobeam has many distinct facets. As we consider the existence of infinite vibrational modes, we are forced to perform a renormalization. Treating this renormalization in a way analogous to the quantization of the electromagnetic field, we have a thermal, or phonon Casimir effect. Also, as a consequence of the infinite vibrational modes, we observe that, depending on the boundary condition, there may be a degeneracy in the Hamiltonian spectrum. The degeneracy ends up having other consequences. For dispersive baths, we observe that there are decoherence-free subspaces; these spaces still exist approximately even when we change the boundary conditions; these are the quasi-degenerate states. For these cases, the decoherence time may be orders of magnitude shorter, so they are possible candidates for use in quantum computing applications.

ACKNOWLEDGMENTS

This work was supported by the Fundação de Amparo à Pesquisa do Estado de Minas Gerais (FAPEMIG) ; the Coordenação de Aperfeiçoamento de Pessoal de Nível Superior (CAPES); and the National Council for Scientific and Technological Development (CNPq).

---

[1] F. G. S. L. Brandão and G. Gour, Reversible framework for quantum resource theories, Phys. Rev. Lett. **115**, 070503 (2015).

[2] A. Kenfack and K. Życzkowski, Negativity of the Wigner function as an indicator of non-classicality, Journal of Optics B: Quantum and Semiclassical Optics **6**, 396 (2004).

[3] A. Sinatra, Spin-squeezed states for metrology, Applied Physics Letters **120**, 120501 (2022).

[4] I. I. Arkhipov, A. Barasiński, and J. Svozilík, Negativity volume of the generalized Wigner function as an entanglement witness for hybrid bipartite states, Sci. Rep. **8**, 1 (2018).

[5] O. Cohen, Nonlocality of the original Einstein-Podolsky-Rosen state, Phys. Rev. A **56**, 3484 (1997).

[6] K. Banaszek and K. Wodkiewicz, Nonlocality of the Einstein-Podolsky-Rosen state in the phase space, Acta Physica Slovaca **49** (1999).

[7] P. M. Anisimov, G. M. Raterman, A. Chiruvelli, W. N. Plick, S. D. Huver, H. Lee, and J. P. Dowling, Quantum metrology with two-mode squeezed vacuum: Parity detection beats the Heisenberg limit, Phys. Rev. Lett. **104**, 103602 (2010).

[8] J. Yin, Y.-H. Li, S.-K. Liao, M. Yang, Y. Cao, L. Zhang, J.-G. Ren, W.-Q. Cai, W.-Y. Liu, S.-L. Li, R. Shu, Y.-M. Huang, L. Deng, L. Li, Q. Zhang, N.-L. Liu, Y.-A. Chen, C.-Y. Lu, X.-B. Wang, F. Xu, J.-Y. Wang, C.-Z. Peng, A. K. Ekert, and J.-W. Pan, Entanglement-based secure quantum cryptography over 1,120 kilometres, Nature **582**, 501 (2020).

[9] N. Shiraishi and R. Takagi, Arbitrary amplification of quantum coherence in asymptotic and catalytic transformation, Phys. Rev. Lett. **132**, 180202 (2024).

[10] A. C. Oliveira, A. B. de Magalhães, and J. P. de Faria, Influence of experimental resolution on the quantum-to-classical transition in the quartic oscillator, Physica A: Statistical Mechanics and its Applications **391**, 5082 (2012).

[11] A. C. Oliveira, Classical limit of quantum mechanics induced by continuous measurements, Physica A: Statistical Mechanics and its Applications **393**, 655 (2014).

[12] V. B. Braginsky, Y. I. Vorontsov, and K. S. Thorne, Quantum nondemolition measurements, Science **209**, 547 (1980), https://www.science.org/doi/pdf/10.1126/science.209.4456.547.

[13] Y. Pan, E. Cohen, E. Karimi, A. Gover, N. Schönenberger, T. Chlouba, K. Wang, S. Nehemia, P. Hommelhoff, I. Kaminer, and Y. Aharonov, Weak measurements and quantum-to-classical transitions in free electron–photon interactions, Light Sci. Appl. **12**, 1 (2023).

[14] M. Brune, E. Hagley, J. Dreyer, X. Maître, A. Maali, C. Wunderlich, J. M. Raimond, and S. Haroche, Observing the progressive decoherence of the "meter" in a quantum measurement, Phys. Rev. Lett. **77**, 4887 (1996).

[15] S. Takahashi, I. S. Tupitsyn, J. van Tol, C. C. Beedle, D. N. Hendrickson, and P. C. E. Stamp, Decoherence in crystals of quantum molecular magnets, Nature **476**, 76 (2011).

[16] M. Korobko, J. Südbeck, S. Steinlechner, and R. Schnabel, Mitigating quantum decoherence in force sensors by internal squeezing, Phys. Rev. Lett. **131**, 143603 (2023).

[17] S. Etaki, M. Poot, I. Mahboob, K. Onomitsu, H. Yamaguchi, and H. S. J. van der Zant, Motion detection of a micromechanical resonator embedded in a d.c. SQUID, Nat. Phys. **4**, 785 (2008).

[18] A. Eichler, J. Moser, J. Chaste, M. Zdrojek, I. Wilson-Rae, and A. Bachtold, Nonlinear damping in mechanical resonators made from carbon nanotubes and graphene, Nat. Nanotechnol.

6, 339 (2011).

[19] H. Stuart, Quantum computation in brain microtubules? The Penrose–Hameroff 'Orch OR' model of consciousness, Philos. Trans. R. Soc. London, Ser. A **356**, 1869 (1998).

[20] R. Y. Brito, D. L. Fabrino, and A. Oliveira, Estudo de Vibrações Mecânicas em Microtúbulos Celulares, Proceedings. of SBMAC **4**, 10.5540/03.2016.004.01.0020 (2016).

[21] Ömer Civalek and Çiğdem Demir, Bending analysis of microtubules using nonlocal euler–bernoulli beam theory, Applied Mathematical Modelling **35**, 2053 (2011).

[22] K. Eom, H. S. Park, D. S. Yoon, and T. Kwon, Nanomechanical resonators and their applications in biological/chemical detection: Nanomechanics principles, Physics Reports **503**, 115 (2011).

[23] M. Poot and H. S. van der Zant, Mechanical systems in the quantum regime, Physics Reports **511**, 273 (2012).

[24] O. Słowik, K. Orłowska, D. Kopiec, P. Janus, P. Grabiec, and T. Gotszalk, Quantum mechanical aspects in the MEMS/NEMS technology, Measurement Automation Monitoring **62**, 87 (2016).

[25] M. Blencowe, Quantum electromechanical systems, Physics Reports **395**, 159 (2004).

[26] R. A. Norte, J. P. Moura, and S. Gröblacher, Mechanical resonators for quantum optomechanics experiments at room temperature, Phys. Rev. Lett. **116**, 147202 (2016).

[27] R. Penrose and S. Hameroff, What 'Gaps'? Reply to Grush and Churchland, Journal of Consciousness Studies **2**, 98 (1995).

[28] J. Awrejcewicz, O. S. ans Y.B. Chebotyrevskiy, and A. Krysko, Nonlinear vibrations of the Euler-Bernoulli beam subject to transversal load and impact actions, Nonlinear Stud. **18** (2011), [Online; accessed 24. Sep. 2025].

[29] S. Zhou, G. Song, Z. Ren, and B. Wen, Nonlinear analysis of a parametrically excited beam with intermediate support by using multi-dimensional incremental harmonic balance method, Chaos, Solitons & Fractals **93**, 207 (2016).

[30] F. Pellicano and F. Vestroni, Nonlinear dynamics and bifurcations of an axially moving beam, Journal of Vibration and Acoustics **122**, 21 (1999).

[31] C. Li-qun, C. Chang-jun, and Z. Neng-hui, Chaotic motion of viscoelastic beams with geometric and physical nonlinearities, Engineering Mechanics **18**, 1 (2001).

[32] Z. Nianmei, Y. Guitong, and X. Bingye, Chaotic belt phenomena in nonlinear elastic beam, in *Advances in Steel Structures (ICASS '99)*, edited by S. Chan and J. Teng (Elsevier, Oxford, 1999) pp. 125–132.

[33] W. Zhang, F. Wang, and M. Yao, Global bifurcations and chaotic dynamics in nonlinear nonplanar oscillations of a parametrically excited cantilever beam, Nonlinear Dyn. **40**, 251 (2005).

[34] Y. Liu, G. Ma, and Q. Li, Chaotic and asymmetrical beam response to impulsive load, International Journal of Solids and Structures **41**, 765 (2004).

[35] H. Norouzi and D. Younesian, Chaotic vibrations of beams on nonlinear elastic foundations subjected to reciprocating loads, Mechanics Research Communications **69**, 121 (2015).

[36] D. Cao and W. Zhang, Global bifurcations and chaotic dynamics for a string-beam coupled system, Chaos, Solitons & Fractals **37**, 858 (2008).

[37] A. Gusso, R. L. Viana, A. C. Mathias, and I. L. Caldas, Nonlinear dynamics and chaos in micro/nanoelectromechanical beam resonators actuated by two-sided electrodes, Chaos, Solitons & Fractals **122**, 6 (2019).

[38] G. V. Soares, D. G. Ladeira, and A. C. Oliveira, Dynamics of a Euler–Bernoulli beam on nonlinear viscoelastic foundations: a parameter space analysis, J. Braz. Soc. Mech. Sci. Eng. **42**, 1 (2020).

[39] M. Alimoradzadeh, Ş. Akbaş, and S. Esfrajani, Nonlinear dynamic and stability of a beam resting on the nonlinear elastic foundation under thermal effect based on the finite strain theory, Structural Engineering and Mechanics **80**, 275 (2021).

[40] R. Rafiee and R. M. Moghadam, On the modeling of carbon nanotubes: A critical review, Composites Part B: Engineering **56**, 435 (2014).

[41] B. I. Yakobson, C. J. Brabec, and J. Bernholc, Nanomechanics of carbon tubes: Instabilities beyond linear response, Phys. Rev. Lett. **76**, 2511 (1996).

[42] A. Kis and A. Zettl, Nanomechanics of carbon nanotubes, Philosophical Transactions: Mathematical, Physical and Engineering Sciences **366**, 1591 (2008).

[43] J.-W. Jiang and J.-S. Wang, Why edge effects are important on the intrinsic loss mechanisms of graphene nanoresonators, Journal of Applied Physics **111**, 054314 (2012).

[44] P. G. Kwiat, A. J. Berglund, J. B. Altepeter, and A. G. White, Experimental verification of decoherence-free subspaces, Science **290**, 498 (2000).

[45] D. A. Lidar, I. L. Chuang, and K. B. Whaley, Decoherence-free subspaces for quantum computation, Phys. Rev. Lett. **81**, 2594 (1998).

[46] A. R. Bosco de Magalhães and M. C. Nemes, Searching for decoherence-free subspaces in cavity quantum electrodynamics, Phys. Rev. A **70**, 053825 (2004).

[47] Q. A. Turchette, C. J. Myatt, B. E. King, C. A. Sackett, D. Kielpinski, W. M. Itano, C. Monroe, and D. J. Wineland, Decoherence and decay of motional quantum states of a trapped atom coupled to engineered reservoirs, Phys. Rev. A **62**, 053807 (2000).

[48] A. C. Oliveira and A. R. B. de Magalhães, Role of the effective Hilbert-space size of the reservoir for the decoherence process, Phys. Rev. E **80**, 026204 (2009).

[49] B. Balachandran and E. Magrab, *Vibrations* (Cengage Learning, 2008).

[50] W. P. Schleich, *Quantum Optics in Phase Space* (Wiley-VCH, 2001).

[51] G. Lee and A. Rodin, Phonon Casimir effect in polyatomic systems, Phys. Rev. B **103**, 195434 (2021).

[52] A. Motazedifard, M. H. Naderi, and R. Roknizadeh, Dynamical Casimir effect of phonon excitation in the dispersive regime of cavity optomechanics, J. Opt. Soc. Am. B **34**, 642 (2017).

[53] M. Schecter and A. Kamenev, Phonon-mediated Casimir interaction between mobile impurities in one-dimensional quantum liquids, Phys. Rev. Lett. **112**, 155301 (2014).

[54] A. S. Dehkharghani, A. G. Volosniev, and N. T. Zinner, Coalescence of two impurities in a trapped one-dimensional Bose gas, Phys. Rev. Lett. **121**, 080405 (2018).

[55] C. C. Gomes, H. C. F. Lemos, and A. C. Oliveira, Semiclassical quantization of Euler-Bernoulli beams: including vacuum effects (2025), in progress.

[56] M. Takamura, H. Okamoto, K. Furukawa, H. Yamaguchi, and H. Hibino, Energy dissipation in graphene mechanical resonators with and without free edges, Micromachines **7**, 10.3390/mi7090158 (2016).

[57] Z. Qi and H. S. Park, Intrinsic energy dissipation in CVD-grown graphene nanoresonators, Nanoscale **4**, 3460 (2012).

[58] A. K. Vallabhaneni, J. F. Rhoads, J. Y. Murthy, and X. Ruan, Observation of nonclassical scaling laws in the quality factors of cantilevered carbon nanotube resonators, Journal of Applied Physics **110**, 034312 (2011).

[59] A. Bosco de Magalhães, S. Mokarzel, M. Nemes, and M. Terra Cunha, Decay rate and decoherence control in coupled dissipative cavities, Physica A: Statistical Mechanics and its Applications **341**, 234 (2004).